Submitted to Catalysis Letters (Revision)

Photodeposition conditions of silver cocatalyst on titanium oxide photocatalyst directing product selectivity in photocatalytic reduction of carbon dioxide with water

Ahmed Hammad,[a,b] Akihiko Anzai,[c] Xing Zhu,[c] Akira Yamamoto,[c,d] Daiki Ootsuki,[c] Teppei Yoshida,[c] Ahmed EL-Shazly,[a] Marwa Elkady[a] and Hisao Yoshida[c,d]

[a.] *Chemical and Petrochemicals Engineering Department, Egypt-Japan University of Science and Technology, New Borg El-Arab City, Alexandria, Egypt.*

[b.] *Chemical Engineering Department, Faculty of Engineering, Port Said University, Port Said, Egypt.*

[c.] *Kyoto University, Graduate School of Human and Environmental Studies, Kyoto 606–8501, Japan.*

[d.] *Kyoto University, Elements Strategy Initiative for Catalysts and Batteries (ESICB), Kyoto 615–8520, Japan.*

Corresponding author:

Hisao YOSHIDA, Professor, Dr.
Material Functions and Correlations
Course of Studies on Material Science
Department of Interdisciplinary Environment
Graduate School of Human and Environmental Studies
Kyoto University
Yoshida-nihonmatsu-cho, Sakyo-ku, Kyoto 606-8501, Japan
Phone: +81-75-753-6594
FAX: +81-75-753-2988
E-mail: yoshida.hisao.2a@kyoto-u.ac.jp

Abstract: Ag-loaded TiO_2 photocatalysts prepared by photodeposition method in an argon atmosphere exhibited highly selective photocatalytic activity for CO_2 reduction with water to produce CO, while the sample prepared under an air atmosphere predominantly promoted water splitting.
Keywords: Photocatalytic CO_2 reduction; Carbon monoxide; Titanium oxide; Silver cocatalyst; Water splitting.

1. Introduction

The increase in the atmospheric CO_2 level as a result of the huge fossil fuels consumption has led researchers trying to find ways to reduce CO_2 concentration [1]. In the last decades, as a new approach for this problem, photocatalytic CO_2 reduction has attracted the researcher's attention since it can convert CO_2 to valuable chemicals or fuels like CO and CH_4 using sunlight [2]. However, this idea has not been for actual use due to low yield and selectivity of the products yet, so the research for useful and reliable photocatalyst for CO_2 reduction is still required [3].

One of the most investigated material in photocatalytic reactions would be titanium dioxide (TiO_2), since it has many advantages such as chemically stable, harmless, ubiquitous, costless, and corrosion-resistant [4]. Titanium dioxide is found in nature in different crystalline phases such as anatase, rutile, and brookite [5]. The most common crystal structures are anatase and rutile, which can be photoexcited by the light of higher energy than each band gap of 3.2 eV and 3.0 eV, respectively [6]. In many cases, anatase showed superior photocatalytic response than rutile owing to its lower recombination rate [7-9], while P-25 (Degussa), a famous commercial TiO_2 product which is a mixture of anatase phase and rutile phase, often illustrated better photocatalytic response than pure rutile or anatase [10,11].

A usual way for improving the photocatalytic response of heterogeneous photocatalysts is noble metal loading, like Pt, Pd, Au, and Ag, as a cocatalyst . Noble metal nanoparticles such as Pt can efficiently receive photoexcited electrons from

the conduction band to decrease recombination of photoexcited electron and hole, resulting in high photocatalytic activity [12-18]. Some kinds of metal nanoparticles showing a localized surface plasmon resonance (LSPR) such as Au can provide plasmonic photocatalysis under visible light [19-23]. Further, in some cases metal nanoparticles such as Pd and Ag can catalyze a certain step in the photocatalytic reactions [24-27].

In photocatalytic CO_2 reduction with water, cocatalyst can determine the product selectivity: Pt, Au, and Cu cocatalysts give favorably CH_4 [28-30], while Ag cocatalysts tends to form CO preferably [31-44]. Ag cocatalyst on various materials have been reported for photocatalytic CO_2 reduction with water recently, like Ag/ $ALa_4Ti_4O_{15}$ (A = Ca, Sr, and Ba) [31], Ag/$KCaSrTa_5O_{15}$ [32], Ag/Ga_2O_3 [33,34], Ag/$SrNb_2O_6$ [35], Ag/$CaTiO_3$ [36,37], and Ag/$Na_2Ti_6O_{13}$ [38,39]. These materials can convert CO_2 to CO by using water as an electron donor and the selectivity between H_2 and CO as reductive products has been discussed since both photocatalytic CO_2 reduction and water splitting can take place competitively.

In this study, photocatalytic CO_2 reduction by Ag-loaded TiO_2 photocatalyst (Ag/TiO_2) was investigated, which have been reported to produce CO [40-44] or CH_4 [45,46] as gaseous products. This means that the state of Ag cocatalyst, the preparation method and so on would determine the product selectivity. So far, many preparation methods of Ag/TiO_2 were reported such as simple silver mirror reaction [40], a microwave-assisted chemical reduction [41], cold plasma [42], hydrothermal treatment [43], electrospinning method [44], electrochemical deposition method [45], and photo-deposition [46]. Among them, the photodeposition method is the most popular and unique method for the preparation of photocatalyst. In this method, Ag cations as the precursor in aqueous solution are reduced by photoexcited electrons to form metallic Ag nanoparticles on TiO_2 surface. In this

process, air is usually not welcomed since molecular oxygen easily consume the photoexcited electron.

Here, we found that the property of the Ag cocatalyst on TiO_2 photocatalyst drastically varies with the atmosphere during the photodeposition procedure: the photocatalysts prepared in an argon atmosphere showed high selectivity for CO_2 reduction, while the sample prepared under an air atmosphere predominantly promoted water splitting.

2. Experimental

2.1. Sample preparation

Ag-loaded TiO_2 (Ag/TiO_2) samples were prepared with alternative photo-deposition methods. Four types of TiO_2 samples were employed from JRC (Japan reference catalysts) samples; JRC-TIO-1 (anatase), JRC-TIO-4 (mixture of anatase and rutile, equivalent to P25), JRC-TIO-6 (rutile), and JRC-TIO-14 (anatase), with a specific surface area of 75, 50, 100, and 338 m^2g^{-1}, respectively. In method A, a suspension of 1 g of TiO_2 powder in 300 ml of aqueous solution of $AgNO_3$ in a beaker was magnetically stirred for 10 min, photoirradiated from the top side with a ceramic xenon lamp (PE300BUV, 300 W) for 120 min under continuous stirring in the air atmosphere, and filtered, followed by washing and drying in an electric oven at 373 K for 12 h and then grounded, which is referred to as Ag(*x*)/TiO_2(A,*y*), where *x* presents loading amount of Ag in weight %, A means this method A, and if any, *y* shows the code number of TiO_2 sample (JRC-TIO-*y*). In method B, 1 g of TiO_2 sample (JRC-TIO-4) was suspended in 1800 ml of an aqueous solution of $AgNO_3$ (desired concentration) and $NaHCO_3$ (0.1 mol L^{-1}) in a quartz reactor with bubbling flow of argon for 1 h at 60 ml min^{-1} to ensure no oxygen gas remained in the reactor, photoirradiated from the center of the reactor with a high pressure Hg lamp (400W) for 120 min under continuous stirring, and successively used for the photocatalytic

reaction test for CO_2 reduction. The samples are referred to as Ag(*x*)/TiO_2(B,4), where B indicates the method B.

2.2. Characterization

Diffuse reflectance (DR) UV-visible spectra were recorded on a V-670 (JASCO) equipped with an integrating sphere covered with $BaSO_4$. X-ray photoelectron spectroscopy (XPS) was conducted using Al Kα X-ray source (12 kV, 1486.6 eV) and hemispherical multichannel analyser (VSM), where binding energy was calibrated with respect to Au $4f_{7/2}$ core level at 83.9 eV. The TEM image of the sample put on a carbon coated copper grid was obtained by a JEM-2100F (JEOL) at an acceleration voltage of 200 kV. Elemental mapping was obtained by EDX in the TEM operating at 200 kV (Oxford Instruments INCA EDS 80 mm X-Max detector).

2.3. Photocatalytic reaction test

Photocatalytic CO_2 reduction test was carried out in an inner irradiation photochemical reactor equipped with a 400 W high pressure Hg lamp. In the reactor, 1 g of photocatalyst sample was suspended in 1800 ml water with $NaHCO_3$ (0.1 mol L^{-1}) and CO_2 bubbling (60 mL min^{-1}) for 2 h to remove air, followed by photoirradiation for 6 h. The outlet gaseous products were analyzed by a gas chromatograph (Shimadzu GC-8A, TCD), where carbon monoxide, oxygen, hydrogen and a small amount of methane were detected.

3. Results and discussion

3.1 Characterizations

Fig. 1A illustrates DR UV-visible spectra of the four kinds of JRC TiO_2 samples loaded with 1% Ag by the method A. The Ag(1)/TiO_2(A,4) and Ag(1)/TiO_2(A,14) samples showed a broad LSPR (localized surface plasmon resonance) band, showing the existence of Ag metallic nanoparticles. Especially, the Ag(1)/TiO_2(A,4) sample

exhibited a large band, meaning a larger number of Ag metallic nanoparticles. In Fig. 1B, DR UV-vis spectra of JRC-TIO-4 samples prepared by the method A with different Ag loading are presented. Among them, the samples with low loading amount (1–3 wt%) of Ag exhibited a clear LSPR peak, indicating that small loading provides Ag nanoparticles responsible to the LSPR. The samples with high loading amount (4–5 wt%) gave a small and broad LSPR band shifted to longer wavelength side, suggesting that the size of Ag nanoparticles became bigger with increasing the loading amount. Fig. 1C shows the spectra of the samples prepared by the method B. Every sample exhibited a large LSPR band. Although the band position and intensity varied with increasing loading amount and the variation was somewhat complex, the LSPR bands were clearly observed on the samples prepared by the method B even for the higher loading samples compared to the samples prepared by the method A. This implies that the larger number of small Ag nanoparticles exist on the samples prepared by the method B. This can be explained by the difference of the preparation method. In the method A, Ag^+ ions and molecular oxygen from air would competitively be reduced by the photoexcited electron, which would decrease the reduction rate of Ag^+ and a large number of Ag^+ would be reduced on the surface of the initially produced Ag nanoparticles. This should make the Ag particle larger. In method B, the Ag species would tend to be directly reduced by the photoexcitaed electrons on the TiO_2 surface without such competition, which can initially provide a large number of smaller nanoparticles deposited on the TiO_2 surface.

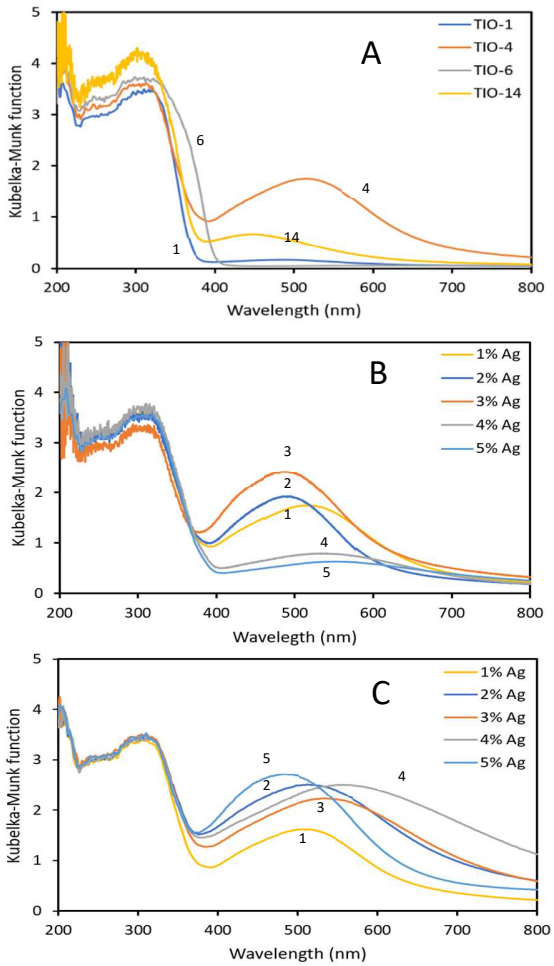

Fig. 1 DR UV-vis spectra of Ag/TiO_2 samples. (A) Ag(1)/TiO_2(A,*y*), various TiO_2 samples loaded with 1% Ag photodeposited by method A, (B) Ag(*x*)/TiO_2(A,4), TIO-4 samples with different silver loading photodeposited by method A, and (C) Ag(*x*)/TiO_2(B,4), TIO-4 samples with different silver loading photodeposited by method B.

Fig. 2 illustrates the TEM images of the Ag(2)/TiO_2(A,4) and Ag(2)/TiO_2(B,4) samples. The particles of 20–50 nm in size correspond to TiO_2 particles in JRC-TIO-4 and small dark dots around 2–3 nm in size would be assigned to Ag nanoparticles. The Ag nanoparticles were well dispersed the TiO_2 particles, and could be observed more clearly on the Ag(2)/TiO_2(A,4) samples in the TEM images.

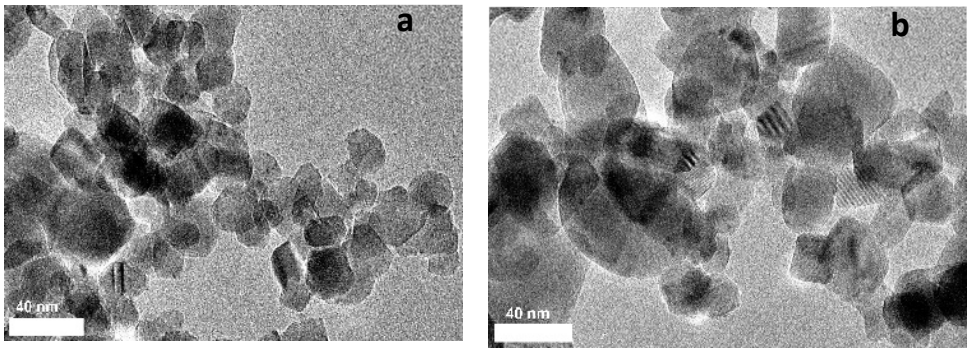

Fig. 2 TEM images of (a) the Ag(2)/TiO_2(A,4) sample and (b) the Ag(2)/TiO_2(B,4) sample.

Energy dispersive x-ray (EDX) mappings of these samples (Fig. S1 and S2) revealed that the Ag species were well distributed in the Ag(2)/TiO_2(A,4) sample (Fig. S1b), while many Ag species were inhomogeneously present in the Ag(2)/TiO_2(B,4) sample (Fig. S2b). From the EDX, the actual loading amount of Ag species was calculated to be 0.59 and 2.1 wt% for the Ag(2)/TiO_2(A,4) and Ag(2)/TiO_2(B,4) samples, respectively. This means that the presence of molecular oxygen during the photodeposition is not suitable for quantitative loading of Ag ions on TiO_2 surface from the aqueous solution (method A), while the condition free from molecular oxygen is suitable for quantitative deposition of Ag species (method B).

XPS analysis was carried out for the Ag(2)/TiO_2 samples prepared by the method A and B and the bare JRC-TIO-4 sample. The photoelectron bands from Ag $3d_{5/2}$ were observed at 368.7 eV (Fig. 3Aa) and 368.5 eV (Fig. 3Ab) for the samples prepared by the A and B methods, respectively, where the former sample showed slightly larger binding energy and the difference was as small as 0.2 eV. In literature, binding energies of Ag $3d_{5/2}$ for Ag and Ag_2O are reported as 368.1 and 367.7 eV, respectively [47,48], and the difference is 0.4 eV. In silver oxide system, it has been known that the binding energy of Ag $3d_{5/2}$ peak exhibits a negative shift as the oxidation state increased and the investigation of the exact oxidation state are not easy due to the

high reactivity of Ag species to oxygen or carbon dioxide in air [49]. The present result suggests that the Ag species are rather metallic in the Ag(2)/TiO_2(A,4) sample and rather oxidized in the Ag(2)/TiO_2(B,4) sample. The Ag species in the present samples would be oxidized since they were exposed in air for a long time before the XPS measurements. Here, it can be noted that the Ag(2)/TiO_2(A,4) sample exhibited broader band width as shown in Fig. 3B, suggesting the wider distribution of the oxidation state including both metallic and oxidized states. These facts consisted with the size distribution of Ag nanoparticles proposed from the UV-vis spectra. The sample prepared by the method A having larger size of Ag nanoparticles would be partially oxidized from the surface by air exposure and the distribution of oxidation state would be wide. In the sample prepared by the method B containing the smaller Ag nanoparticles, the Ag species would be fully oxidized in air.

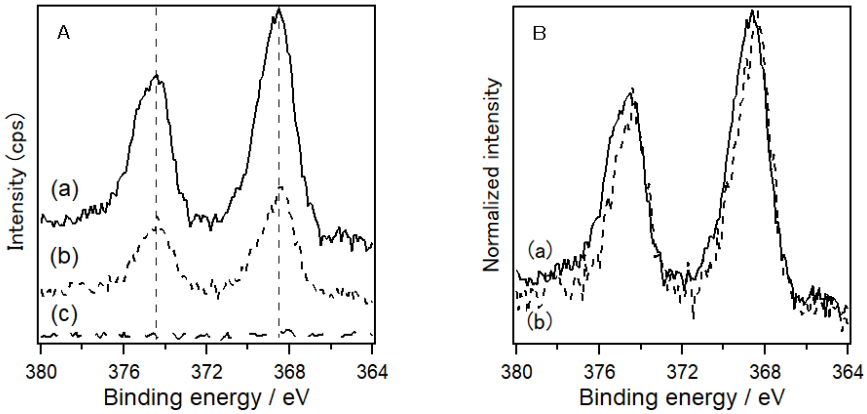

Fig. 3 Ag $3d_{5/2}$ XPS spectra of (a) the Ag(2)/TiO_2(A,4) sample, (b) the Ag(2)/TiO_2(B,4) sample, and (c) the bare JRC-TIO-4 sample.

From these results of characterizations, the states of deposited Ag species on the samples prepared by the alternative methods were similar to but slightly different

from each other. The samples prepared by the method B had larger number of small Ag nanoparticles.

3.2 Photocatalytic activities

Photocatalytic performance of these samples were examined for the photocatalytic CO_2 reduction with water. The production rates of dominant gaseous products, H_2, CO and O_2, were shown in Fig. 4, where H_2 and CO were the products in water splitting and CO_2 reduction, respectively. In these experiments O_2 as a common product in both the reactions was also detected although the amount did not consist with the expected one from the ideal stoichiometric ratio, which would originate from some reasons discussed in our previous study [38].

The first set of the tests were conducted with Ag(1)/TiO_2 samples prepared by the method A by using various kinds of TiO_2, as shown in Fig. 4A. All the samples produced H_2 as a main product, where the Ag-loaded JRC-TIO-4 sample exhibited a higher CO production rate than the other three samples. It is noticed that the order of the SPR band intensity in the visible light region of the DR UV-visible spectra (Fig. 1A) seems to be the same order of the CO formation rate, suggesting that the state of the Ag species as nanoparticles much contributes to the high CO formation rate and selectivity. Between the two anatase samples, the one having higher specific surface area exhibited more intense LSPR band and higher photocatalytic activity to form H_2 and CO, where the selectivity to CO (S_{CO}) was of the similar level around 13%. Among the four samples, the TiO_2 sample consisting of anatase and rutile nanoparticles seems to be most suitable to form Ag nanoparticles showing the largest LSPR band and to produce CO with the high selectivity of S_{CO}=33.5%. Thus, photocatalytic CO_2 reduction tests were conducted with the Ag-loaded JRC-TIO-4 samples hereinafter.

The bare JRC-TIO-4 sample without deposition of Ag cocatalyst showed very low CO production rate (0.434 μmol h^{-1}), which confirms that Ag nanoparticles are necessary to produce CO. The results of the samples with various amount of Ag cocatalyst prepared by the methods A and B are as shown in Fig. 4B and 4C, respectively. At a glance, it is obviously shown that the Ag(*x*)/TiO_2(B,4) photocatalyst prepared by the method B produced predominantly CO and less hydrogen, where the CO selectivity S_{CO} achieved over 80% (Fig. 4C), while the Ag(*x*)/TiO_2(A,4) photocatalyst prepared by the method A gave H_2 mainly with less CO selectivity less than 50% (Fig. 4B). Especially, the Ag(2)/TiO_2(B,4) showed the highest CO production rate 11.5 μmol h^{-1} with high CO selectivity (S_{CO}=80%). Further increase of Ag over 3 wt% decreased the photocatalytic activity although they maintained similar CO selectivity over 80%. This is due to agglomeration of Ag nanoparticles deposited on the TiO_2 surface without changing the cocatalyst property to produce CO selectively. The photodeposition by the method B would be suitable for the fabrication of such Ag nanoparticles as a cocatalyst for the selective CO production. The photodeposition condition free from molecular oxygen would preferably promote the reduction of Ag cations by photoexcited electrons to form and deposit small Ag metallic nanoparticles on the TiO_2 surface. The contribution of small size of Ag nanoparticles for CO_2 reduction to CO consists with the literature [33]. In addition, the direct use of the obtained Ag(*x*)/TiO_2(B,4) photocatalyst for the photocatalytic reaction test successively without exposure to the air atmosphere would also contribute to the selective photocatalytic CO_2 reduction to produce CO.

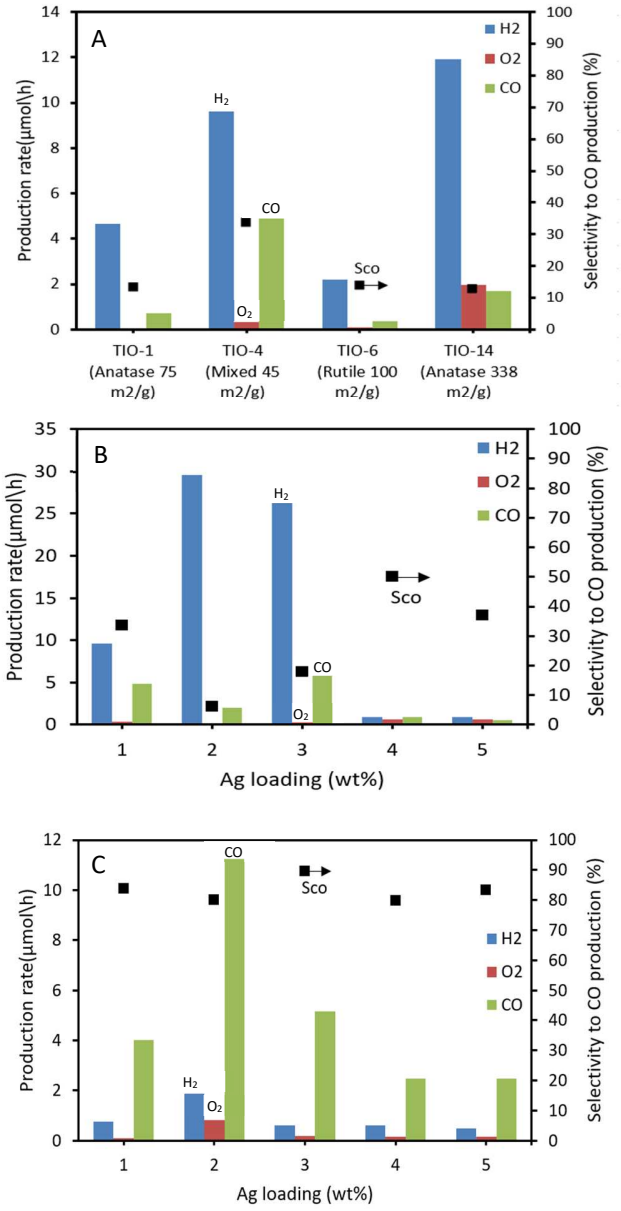

Fig. 4 Production rates of H_2, O_2 and CO and selectivity to CO (S_{CO}) in photocatalytic CO_2 reduction tests with various Ag(x)/TiO_2 samples: (A) the Ag(1)/TiO_2(A,y) samples with four kinds of TiO_2, (B) the Ag(x)/TiO_2(A,4) samples prepared by the method A, (C) the Ag(x)/TiO_2(B,4) samples prepared by the method B.

3.3 Photocatalytic reaction mechanism

Although the reaction mechanism was not investigated in the present study, the outline of the reaction mechanism is mentioned here [50-53]. It is known that once light incidents on the TiO_2 photocatalyst, electrons in a valence band are excited to a conduction band with the formation of positively charged holes in the valence band as shown in Fig. 5. The photoexcited electrons reduce CO_2 to CO (eq. 1) or reduce proton (H^+) to H_2 (eq. 2), while positive holes oxidize H_2O to O_2 (eq. 3)

$$CO_2 + 2H^+ + 2e^- \rightarrow CO + H_2O \qquad (1)$$

$$2H^+ + 2e^- \rightarrow H_2 \qquad (2)$$

$$H_2O + 2h^+ \rightarrow 2H^+ + ½\ O_2 \qquad (3)$$

The small Ag cocatalyst deposited by the method B preferably enhances the photocatalytic CO_2 reduction to form CO (eq. 1), while the large Ag cocatalyst prepared by the method A dominantly enhances the reduction of protons to form hydrogen (eq. 2). Thus, although both photocatalytic CO_2 reduction and water splitting take place competitively, the property of the Ag cocatalyst can direct the reaction selectivity. The possible roles of the Ag cocatalyst discussed so far are as follows: Ag species can efficiently receive the photoexcited electrons from the conduction band of TiO_2, LSPR of the metallic Ag nanoparticles can enhance the photoabsorption or the surface reaction, or the Ag nanoparticles can function as a catalyst to accelerate the reduction of CO_2 and desorption of CO.

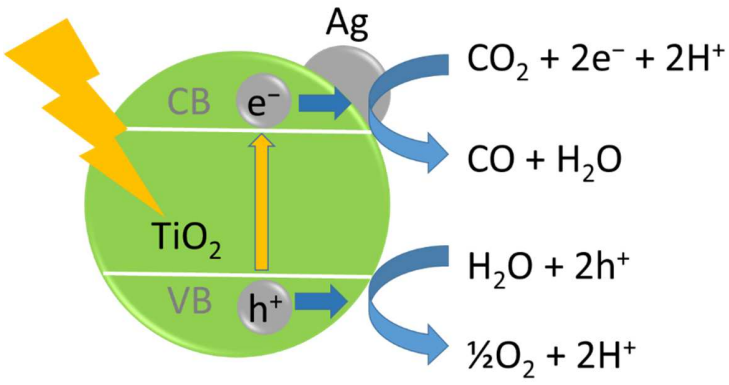

Fig. 5 Proposed mechanism of photocatalytic CO_2 reaction to CO with water on Ag-loaded TiO_2 photocatalyst under UV-vis light irradiation.

4. Conclusions

In the present study, we examined to prepare Ag/TiO_2 photocatalysts by two different photodeposition methods and successfully found a photodeposition method to prepare suitable Ag/TiO_2 photocatalysts for the photocatalytic CO_2 reduction to CO. The obtained Ag/TiO_2 photocatalyst had preferably small Ag nanoparticles on the surface and showed high CO production rate (11.5 μmol h^{-1}) and high CO selectivity (80%).

Conflicts of interest

No conflict of interest.

Acknowledgements

The author, A.S Hammad, gratefully acknowledges the Egyptian Ministry of Higher Education MOHE, which has granted him a full Ph.D. scholarship, and Egypt-Japan University (E-JUST), specially the TMD (Technology Management Department), for providing the facilities to accomplish this work. Additionally, the authors gratefully

acknowledge all members of the Yoshida Lab, Kyoto University for the help and support they offered. This study was financially supported by a Grant-in-Aid for Scientific Research on Innovative Areas “singularity-structure project” (No. 17H05334) from JSPS, and the Program for Element Strategy Initiative for Catalysts & Batteries (ESICB), commissioned by the MEXT of Japan.

References

1. Ekwurzel B, Boneham J, Dalton MW, et al (2017) The rise in global atmospheric CO_2, surface temperature, and sea level from emissions traced to major carbon producers. Clim Change 144:579–590. https://doi.org/10.1007/s10584-017-1978-0
2. Jiang Z, Xiao T, Kuznetsov VL, Edwards PP (2010) Turning carbon dioxide into fuel. Philos Trans R Soc A Math Phys Eng Sci. 368:3343–3364. https://doi.org/10.1098/rsta.2010.0119
3. Liu L, Li Y (2014) Understanding the reaction mechanism of photocatalytic reduction of CO_2 with H_2O on TiO_2-based photocatalysts: A review. Aerosol Air Qual Res 14:453–469. https://doi.org/10.4209/aaqr.2013.06.0186
4. Pelaez M, Nolan NT, Pillai SC, et al (2012) A review on the visible light active titanium dioxide photocatalysts for environmental applications. Appl Catal B Environ 125:331–349. https://doi.org/10.1016/j.apcatb.2012.05.036
5. Hanaor DAH, Sorrell CC (2011) Review of the anatase to rutile phase transformation. J Mater Sci 46:855–874. https://doi.org/10.1007/s10853-010-5113-0
6. Luttrell T, Halpegamage S, Tao J, et al (2015) Why is anatase a better photocatalyst than rutile? - Model studies on epitaxial TiO_2 films. Sci Rep 4:1–8. https://doi.org/10.1038/srep04043

7. Riegel G, Bolton JR (2005) Photocatalytic efficiency variability in TiO_2 particles. J Phys Chem 99:4215–4224. https://doi.org/10.1021/j100012a050
8. Hurum DC, Agrios AG, Gray KA, Rajh T, Thurnauer MC (2003) Explaining the enhanced photocatalytic activity of Degussa P25 mixed-phase TiO_2 using EPR. J Phys Chem B 107:4545–4549
9. Sclafani A, Herrmann JM (1996) Comparison of the photoelectronic and photocatalytic activities of various anatase and rutile forms of titania in pure liquid organic phases and in aqueous solutions. J Phys Chem 100:13655–13661. https://doi.org/10.1021/jp9533584
10. Amano F, Yasumoto T, Prieto-Mahaney OO, et al (2009) Photocatalytic activity of octahedral single-crystalline mesoparticles of anatase titanium(iv) oxide. Chem Commun 2311–2313. https://doi.org/10.1039/b822634b
11. Spurr RA, Myers H (1957) Quantitative analysis of anatase-rutile mixtures with an X-ray diffractometer. Anal Chem 29:760–762. https://doi.org/10.1021/ac60125a006
12. Yoshida H, Hirao K, Nishimoto JI, et al (2008) Hydrogen production from methane and water on platinum loaded titanium oxide photocatalysts. J Phys Chem C 112:5542–5551. https://doi.org/10.1021/jp077314u
13. Shimura K, Kato S, Yoshida T, et al (2010) Photocatalytic steam reforming of methane over sodium tantalate. J Phys Chem C 114:3493–3503. https://doi.org/10.1021/jp902761x
14. Yuzawa H, Mori T, Itoh H, Yoshida H (2012) Reaction mechanism of ammonia decomposition to nitrogen and hydrogen over metal loaded titanium oxide photocatalyst. J Phys Chem C 116:4126–4136. https://doi.org/10.1021/jp209795t
15. Yuzawa H, Yoshida H (2013) Direct functionalization of aromatic rings on platinum-loaded titanium oxide photocatalyst. Chem Lett 42:1336–1343. https://doi.org/10.1246/cl.130757
16. Yamamoto A, Mizuba S, Saeki Y, Yoshida H (2016) Platinum loaded sodium tantalate

photocatalysts prepared by a flux method for photocatalytic steam reforming of methane. Appl Catal A Gen 521:125–132. https://doi.org/10.1016/j.apcata.2015.10.031

17. Tyagi A, Yamamoto A, Yamamoto M, et al (2018) Direct cross-coupling between alkenes and tetrahydrofuran with a platinum-loaded titanium oxide photocatalyst. Catal Sci Technol 8:2546–2556. https://doi.org/10.1039/c8cy00129d
18. Yoshida H, Yamada R, Yoshida T (2019) Platinum cocatalyst loaded on calcium titanate photocatalyst for water splitting in a flow of water vapor. ChemSusChem 12:1958–1965. https://doi.org/10.1002/cssc.201802799
19. An C, Wang R, Wang S, Zhang X (2011) Converting AgCl nanocubes to sunlight-driven plasmonic AgCl:Ag nanophotocatalyst with high activity and durability. J Mater Chem 21:11532–11536. https://doi.org/10.1039/c1jm10244c
20. Yuzawa H, Yoshida T, Yoshida H (2012) Gold nanoparticles on titanium oxide effective for photocatalytic hydrogen formation under visible light. Appl Catal B Environ 115–116:294–302. https://doi.org/10.1016/j.apcatb.2011.12.029
21. Liu H, Meng X, Dao TD, et al (2015) Conversion of carbon dioxide by methane reforming under visible-light irradiation: Surface-plasmon-mediated nonpolar molecule activation. Angew Chem Int Ed 54:11545–11549. https://doi.org/10.1002/anie.201504933
22. Zhang Q, Mao M, Li Y, et al (2018) Novel photoactivation promoted light-driven CO_2 reduction by CH_4 on Ni/CeO_2 nanocomposite with high light-to-fuel efficiency and enhanced stability. Appl Catal B Environ 239:555–564. https://doi.org/10.1016/j.apcatb.2018.08.052
23. Takami D, Ito Y, Kawaharasaki S, et al (2019) Low temperature dry reforming of methane over plasmonic Ni photocatalysts under visible light irradiation. Sustain Energy Fuels 2:2–5. https://doi.org/10.1039/c9se00206e
24. Yoshida H, Fujimura Y, Yuzawa H, et al (2013) A heterogeneous palladium catalyst

hybridised with a titanium dioxide photocatalyst for direct C-C bond formation between an aromatic ring and acetonitrile. Chem Commun 49:3793–3795. https://doi.org/10.1039/c3cc41068d

25. Tyagi A, Matsumoto T, Kato T, Yoshida H (2016) Direct C-H bond activation of ethers and successive C-C bond formation with benzene by a bifunctional palladium-titania photocatalyst. Catal Sci Technol 6:4577–4583. https://doi.org/10.1039/c5cy02290h
26. Wada E, Takeuchi T, Fujimura Y, et al (2017) Direct cyanomethylation of aliphatic and aromatic hydrocarbons with acetonitrile over a metal loaded titanium oxide photocatalyst. Catal Sci Technol 7:2457–2466. https://doi.org/10.1039/c7cy00365j
27. Tyagi A, Yamamoto A, Kato T, Yoshida H (2017) Bifunctional property of Pt nanoparticles deposited on TiO_2 for the photocatalytic sp^3C-sp^3C cross-coupling reactions between THF and alkanes. Catal Sci Technol 7:2616–2623. https://doi.org/10.1039/c7cy00535k
28. Xie S, Wang Y, Zhang Q, et al (2014) MgO- and Pt-promoted TiO_2 as an efficient photocatalyst for the preferential reduction of carbon dioxide in the presence of water. ACS Catal 4:3644–3653. https://doi.org/10.1021/cs500648p
29. Hou W, Hung WH, Pavaskar P, et al (2011) Photocatalytic conversion of CO_2 to hydrocarbon fuels via plasmon-enhanced absorption and metallic interband transitions. ACS Catal 1:929–936. https://doi.org/10.1021/cs2001434
30. Ambrožová N, Reli M, Šihor M, et al (2018) Copper and platinum doped titania for photocatalytic reduction of carbon dioxide. Appl Surf Sci 430:475–487. https://doi.org/10.1016/j.apsusc.2017.06.307
31. Iizuka K, Wato T, Miseki Y, et al (2011) Photocatalytic reduction of carbon dioxide over Ag cocatalyst-loaded $ALa_4Ti_4O_{15}$ (A = Ca, Sr, and Ba) using water as a reducing reagent. J Am Chem Soc 15:20863–20868
32. Takayama T, Tanabe K, Saito K, et al (2014) The $KCaSrTa_5O_{15}$ photocatalyst with tungsten bronze structure for water splitting and CO_2 reduction. Phys Chem Chem

Phys 16:24417–24422. https://doi.org/10.1039/c4cp03892d

33. Yamamoto M, Yoshida T, Yamamoto N, et al (2015) Photocatalytic reduction of CO_2 with water promoted by Ag clusters in Ag/Ga_2O_3 photocatalysts. J Mater Chem A 3:16810–16816. https://doi.org/10.1039/C5TA04815J
34. Pang R, Teramura K, Tatsumi H, et al (2018) Modification of Ga_2O_3 by an Ag-Cr core-shell cocatalyst enhances photocatalytic CO evolution for the conversion of CO_2 by H_2O. Chem Commun 54:1053–1056. https://doi.org/10.1039/c7cc07800e
35. Xie S, Wang Y, Zhang Q, et al (2015) $SrNb_2O_6$ nanoplates as efficient photocatalysts for the preferential reduction of CO_2 in the presence of H_2O. Chem Commun 51:3430–3433. https://doi.org/10.1039/c4cc10241j
36. Yoshida H, Zhang L, Sato M, et al (2015) Calcium titanate photocatalyst prepared by a flux method for reduction of carbon dioxide with water. Catal Today 251:132–139. https://doi.org/10.1016/j.cattod.2014.10.039
37. Anzai A, Fukuo N, Yamamoto A, Yoshida H (2017) Highly selective photocatalytic reduction of carbon dioxide with water over silver-loaded calcium titanate. Catal Commun 100:134–138. https://doi.org/10.1016/j.catcom.2017.06.046
38 Zhu X, Anzai A, Yamamoto A, Yoshida H (2019) Silver-loaded sodium titanate photocatalysts for selective reduction of carbon dioxide to carbon monoxide with water. Appl Catal B Environ 243:47–56. https://doi.org/10.1016/j.apcatb.2018.10.021
39. Yoshida H, Sato M, Fukuo N, et al (2018) Sodium hexatitanate photocatalysts prepared by a flux method for reduction of carbon dioxide with water. Catal Today 303:296–304. https://doi.org/10.1016/j.cattod.2017.09.029
40. Yu B, Zhou Y, Li P, et al (2016) Photocatalytic reduction of CO_2 over Ag/TiO_2 nanocomposites prepared with a simple and rapid silver mirror method. Nanoscale 8:11870–11874. https://doi.org/10.1039/c6nr02547a
41. Liu E, Kang L, Wu F, et al (2014) Photocatalytic reduction of CO_2 into methanol over

Ag/TiO_2 nanocomposites enhanced by surface plasmon resonance. Plasmonics 9:61–70. https://doi.org/10.1007/s11468-013-9598-7

42. Cheng X, Dong P, Huang Z, et al (2017) Green synthesis of plasmonic Ag nanoparticles anchored TiO_2 nanorod arrays using cold plasma for visible-light-driven photocatalytic reduction of CO_2. J CO2 Util 20:200–207. https://doi.org/10.1016/j.jcou.2017.04.009
43. Li X, Zhuang Z, Li W, Pan H (2012) Photocatalytic reduction of CO_2 over noble metal-loaded and nitrogen-doped mesoporous TiO_2. Appl Catal A Gen 429–430:31–38. https://doi.org/10.1016/j.apcata.2012.04.001
44. Xu F, Meng K, Cheng B, et al (2019) Enhanced photocatalytic activity and selectivity for CO_2 reduction over a TiO_2 nanofibre mat using Ag and MgO as bi-cocatalyst. ChemCatChem 11:465–472. https://doi.org/10.1002/cctc.201801282
45. Low J, Qiu S, Xu D, et al (2018) Direct evidence and enhancement of surface plasmon resonance effect on Ag-loaded TiO_2 nanotube arrays for photocatalytic CO_2 reduction. Appl Surf Sci 434:423–432. https://doi.org/10.1016/j.apsusc.2017.10.194
46. Feng S, Wang M, Zhou Y, et al (2015) Double-shelled plasmonic Ag-TiO_2 hollow spheres toward visible light-active photocatalytic conversion of CO_2 into solar fuel. APL Mater 3:104416. https://doi.org/10.1063/1.4930043
47. Hoflund GB, Weaver JF, Epling WS (2002) Ag foil by XPS. Surf Sci Spectra 3:151–156. https://doi.org/10.1116/1.1247777
48. Hoflund GB, Weaver JF, Epling WS (2002) Ag_2O XPS spectra. Surf Sci Spectra 3:157–162. https://doi.org/10.1116/1.1247778
49. Hoflund GB, Hazos ZF, Salaita GN (2000) Surface characterization study of Ag, AgO, and Ag_2O using x-ray photoelectron spectroscopy and electron energy-loss spectroscopy. Phys Rev B - Condens Matter Mater Phys 62:11126–11133. https://doi.org/10.1103/PhysRevB.62.11126

50. White JL, Baruch MF, Pander JE, et al (2015) Light-driven heterogeneous reduction of carbon dioxide: Photocatalysts and photoelectrodes. Chem Rev 115:12888–12935. https://doi.org/10.1021/acs.chemrev.5b00370

51. Nahar S, Zain MFM, Kadhum AAH, et al (2017) Advances in photocatalytic CO_2 reduction with water: A review. Materials (Basel) 10:629. https://doi.org/10.3390/ma10060629

53. Méndez-Medrano MG, Kowalska E, Lehoux A, et al (2016) Surface modification of TiO_2 with Ag nanoparticles and CuO nanoclusters for application in photocatalysis. J Phys Chem C 120:5143–5154. https://doi.org/10.1021/acs.jpcc.5b10703